Limnol. Oceanogr., 36(8), 1991, 1928–1950

Three-dimensional simulations of the impact of Southern Ocean nutrient depletion on atmospheric CO_2 and ocean chemistry

Jorge L. Sarmiento and James C. Orr
Program in Atmospheric and Oceanic Sciences, Princeton University, Princeton, New Jersey 08544

Abstract

Surface nutrient concentrations in the Southern Ocean are an important indicator of the atmosphere-ocean chemical balance that played a key role in ice-age reduction of atmospheric pCO_2 and would play a role in any Fe fertilization scenario for increasing oceanic uptake of anthropogenic CO_2. The response of the ocean and atmosphere to a scenario of extreme depletion of Southern Ocean surface nutrients by an increase in the organic matter flux to the deep ocean is examined with a three-dimensional model of ocean circulation coupled to a one-box model of the atmosphere. After 100 yr, the increase in the organic matter flux is 6–30 Gt C yr^{-1}—about twice the global new production determined by the same model for the present ocean. The removal of nutrients from surface waters of the Southern Ocean reduces the nutrient content of the near-surface and intermediate depth waters of the entire ocean, resulting in a 0.5–1.9 Gt C yr^{-1} reduction of low-latitude new production. The deep circumpolar waters, enriched in nutrients by regeneration of organic matter, spread into the deep and bottom waters of the remainder of the ocean, giving an overall downward shift of nutrients from surface and intermediate to circumpolar and deep waters. The oceanic total C distribution is also shifted downward, resulting in uptake of atmospheric CO_2 of 46–85 ppm (98–181 Gt C) in the first 100 yr. The oxygen content shifts upward in the water column, approximately mirroring the downward shift of nutrients. Some of the oxygen shifted to the upper ocean escapes to the atmosphere. As a consequence, the global average oceanic content of oxygen, presently 168 μmol kg^{-1}, is reduced by 6–20 μmol kg^{-1}, with anoxia developing in the southwestern Indian Ocean.

CO_2 is unusual compared to other atmospheric gases because most of the combined atmosphere-ocean inventory (98.5%) is in the ocean. By contrast, oxygen, a more typical atmospheric gas, has only 0.6% of its atmosphere-ocean inventory in the ocean. CO_2 is ~30 times as soluble as oxygen, due mainly to hydrogen bonding with water molecules; however, the primary reason for the large amount of CO_2 in the ocean is that it reacts with water to form HCO_3^- and CO_3^{2-}. Only ~1% of the dissolved inorganic C is in the non-ionic CO_2 form (e.g. Broecker and Peng 1982).

Another important contributor to reduced atmospheric CO_2 levels results from the distribution of total inorganic CO_2 (i.e. the sum of the concentrations of CO_2, and HCO_3^- and CO_3^{2-} ions), which is ~12% lower at the surface than at depth. Part of this surface-to-deep difference is due to what is referred to as the "solubility pump" (Volk and Hoffert 1985). CO_2 is more than twice as soluble in the cold, high-latitude waters which sink to form the deep waters of the ocean, than it is in warm, low-latitude waters (Weiss 1974). However, the primary source of the surface to deep difference is the "biological pump" (Volk and Hoffert 1985). Photosynthesis produces organic C from CO_2 in the euphotic zone of the ocean, depleting surface nutrients to near-zero levels over most of the surface ocean. Although most of the photosynthetically produced organic C is recycled in the euphotic zone, ~30% either sinks to the deep ocean or is transported there by circulation before being regenerated to CO_2.

Acknowledgments

This work was supported by the U.S. Department of Energy under contract DEFG 02-90ER61052, by the National Science Foundation (OCE 90-12333), and by GFDL/NOAA through the generosity of K. Bryan and J. Mahlman.

The perturbation approach for modeling total C was developed in collaboration with U. Siegenthaler. The collaboration of J.L.S. with F. Joos and U. Siegenthaler in earlier high-latitude, nutrient-depletion studies gave us considerable insight into how to go about our three-dimensional experiment and how to interpret the results. B. Flannery was the first member of our group to do a nutrient-depletion experiment (summer 1989), following the basic modeling approach developed by R. Najjar. Collaboration of J.C.O. with R. Najjar, R. Slater, and K. Dixon aided in modeling and analysis.

Table 1. Box model scenarios of atmosphere-ocean CO_2 distribution. Full operation of the biological pump corresponds to complete removal of surface nutrients. Partial operation of the biological pump describes the present situation without anthropogenic CO_2 perturbation.

Solubility pump	Biological pump	Atm. pCO_2 (ppm)	Source
No	No	720	Volk and Hoffert 1985
Yes	No	450, 530	Wenk 1985; Bacastow and Maier-Reimer 1990; Baes and Killough 1986
Yes	Partial	280	Neftel et al. 1985
Yes	Full	165	Sarmiento and Toggweiler 1984

Table 1 summarizes results from a series of box model studies that illustrate the sensitivity of atmospheric CO_2 to the solubility and biological pumps. An ocean with no biological pump, and in which the temperature is mixed uniformly so that the solubility pump is inoperative, would have an atmospheric CO_2 level of ~720 ppm, which is more than 2.6 times the preindustrial CO_2 level of 280 ppm. If just the solubility pump were turned on, CO_2 would drop to 450 ppm. If the biological pump were to deplete all surface nutrients, CO_2 would drop to 165 ppm. Thus, the preindustrial CO_2 level of 280 ppm corresponds to the partial operation of the biological pump which we infer from the fact that not all nutrients at the surface of the ocean are depleted (Fig. 1).

Geochemists generally agree that the most likely explanation for the reduced atmospheric CO_2 levels measured in trapped air bubbles formed during the last ice age is that there was a substantial reorganization of oceanic total C and alkalinity distributions (e.g. Broecker 1982; review by Sarmiento et al. 1988; Boyle 1988; Broecker and Peng 1989). The surface nutrient removal hypothesis for the ice ages is based on the suggestion that the biological pump may, under some circumstances, be able to remove a substantial portion of the excess surface nutrients and total C contained in regions such as the Southern Ocean and the North and equatorial Pacific (*see Fig. 1*). It could occur either by weakening of the rate at which nutrients are supplied to the surface or by enhancement of biological production and export of organic matter (Knox and McElroy 1984; Sarmiento and Toggweiler 1984; Siegenthaler and Wenk 1984). Such a reduction of nutrients and total C would decrease the surface ocean pCO_2 resulting in

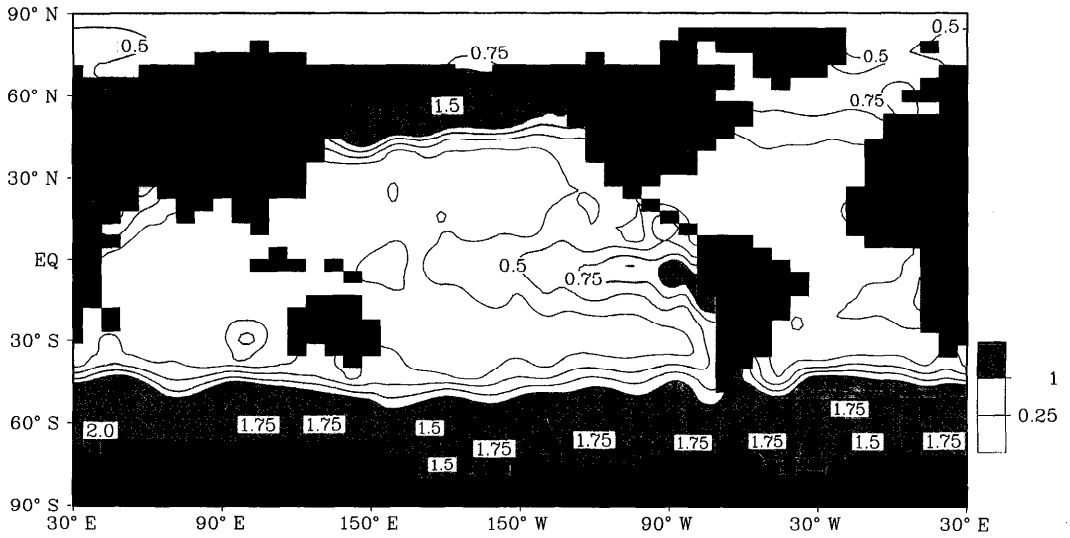

Fig. 1. Phosphate at the surface of the ocean as mapped by S. Levitus and R. G. Najjar (pers. comm.); contour interval is 0.25 μmol kg^{-1}.

uptake of CO_2 from the atmosphere until a new atmosphere-ocean equilibrium was established. The model results discussed here show that the high-nutrient region that is of most importance in controlling atmospheric CO_2 is the Southern Ocean because it serves as a window to the large volume of water contained in the entire deep ocean; in contrast, the North and equatorial Pacific regions are perched on top of isopycnals occupying only a small volume of the ocean.

J. H. Martin has suggested that the present high levels of nutrients in the surface of the Southern Ocean may result from Fe limitation, due to the low atmospheric transport of Fe-containing dust particles to this region (Martin et al. 1990*a,b*). In this view, increased biological export to the deep ocean during the ice age may have resulted from increased atmospheric delivery of dust particles—a phenomenon observed in ice cores (Martin 1990). The iron hypothesis has also led to the intriguing suggestion of fertilizing the present Southern Ocean with Fe as a way of taking up a larger amount of anthropogenic CO_2 than is presently entering the ocean (Martin et al. 1990*a,b*). Estimates of how much CO_2 might be taken up from the atmosphere under such circumstances have been made with box-advection-diffusion models (Peng and Broecker 1991*a,b*; Joos et al. 1991*a,b*). These studies were directed at obtaining an upper limit estimate of the oceanic uptake that might result from complete removal of surface nutrients in the Southern Ocean, assuming it were possible to do this.

We have now succeeded in carrying out a series of three-dimensional oceanic general circulation model studies of the Southern Ocean surface nutrient-depletion scenario. We use a perturbation approach similar to that of Joos et al. (1991*a*), which was developed for three-dimensional model studies of oceanic uptake of anthropogenic CO_2 (Sarmiento et al. 1992). This new three-dimensional study is the basis for our paper.

Model description

We use the PO_4^{3-} budget as an upper limit indicator of how much C might be removed from the surface by the biological pump. We assume, for purposes of this study, that Fe fertilization makes it possible to deplete surface PO_4^{3-} entirely. This assumption ignores other factors that could limit nutrient uptake, such as light supply and zooplankton grazing (e.g. Mitchell 1991; Nelson and Smith 1991; Frost 1991; Cullen 1991). NO_3^- could be used as an upper limit indicator as well, but we prefer, for now, to avoid the problem of dealing with denitrification, N_2 fixation, and other complex processes that contribute to the N cycle.

The first effect of depletion of surface PO_4^{3-} in the Southern Ocean is reduction of C in an amount predicted by the Redfield C:P ratio. This C removal reduces pCO_2 in the surface water, thereby taking up CO_2 from the atmosphere until a new equilibrium is established. That equilibrium would not be established until all the deep water outcropping at the surface in the Southern Ocean had cycled through the surface. Thus, prediction of CO_2 uptake requires solving the conservation equation

$$\frac{\partial C}{\partial t} = -\boldsymbol{V}\cdot\nabla C + \nabla\cdot(\mathbf{D}\nabla C) + SMS_C \quad (1)$$

where C is the concentration of PO_4^{3-} or total C (we also simulate oxygen). $\boldsymbol{V}$ is the velocity vector, $\mathbf{D}$ is the diffusion tensor, and SMS_C is all other sources minus sinks, specifically gas exchange at the surface, and biological uptake and remineralization.

The usual approach to solving Eq. 1 would be to obtain a steady state solution for the preindustrial C and nutrient balance, then use this as an initial condition for a study of the time-dependent response to nutrient depletion in the Southern Ocean (e.g. Peng and Broecker 1991*a*). Following the lead of Joos et al. (1991*a*), we avoid this by assuming that the preindustrial PO_4^{3-}, C, and O_2, symbolized by C_0, were in steady state, i.e. $\partial C_0/\partial t = 0$. Then, by subtracting Eq. 1 for C_0 from Eq. 1 for C, we obtain

$$\frac{\partial \delta C}{\partial t} = -\boldsymbol{V}\cdot\nabla\delta C + \nabla\cdot(\mathbf{D}\nabla\delta C) + \delta SMS_C \quad (2)$$

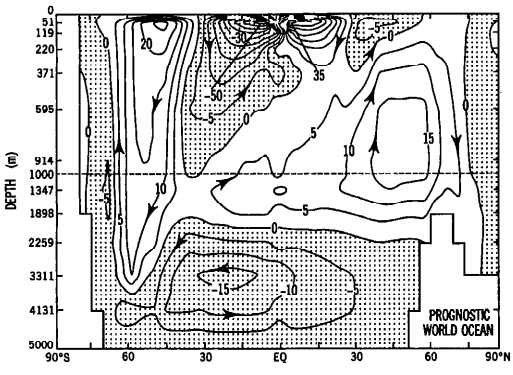

Fig. 2. Zonally integrated meridional overturning in the global ocean model of Toggweiler et al. (1989*a*) in units of 10^6 m^3 s^{-1}.

where $\delta C = C - C_0$ and $\delta SMS_C = SMS_C - SMS_{C_0}$. The initial condition for this equation is $\delta C = 0$, since $C = C_0$ at the beginning of the simulation. In order to solve Eq. 2, we must specify, $\boldsymbol{V}$, **D**, and δSMS (i.e. gas exchange, biological uptake, and remineralization).

Physical processes—We use average advection ($\boldsymbol{V}$) and diffusion (**D**) fields obtained from the nonseasonal prognostic world ocean model developed by Toggweiler et al. (1989*a*, their model P) in an "off-line" solution of the conservation equation only, which avoids the large computational cost of running the full primitive equation set to solve for the velocity field. The diffusion tensor includes convection, which is implemented by homogenizing adjacent layers that become unstably stratified with respect to each other due to buoyancy forcing at the surface or advection of more dense over less dense waters (e.g. Gargett 1991).

Toggweiler et al. (1989*a*) obtained their flow field with the method of Bryan (1969) to solve the equations of motion as modified by the Boussinesq and hydrostatic approximations, as well as the equations of continuity, conservation of salinity and potential temperature, and state. The model has a north-south resolution of 4.5°, an east-west resolution of 3.75°, and a maximum depth of 5,000 m resolved by 12 levels in the vertical (depth level midpoints are 26, 85, 170, 295, 483, 755, 1,131, 1,622, 2,228, 2,935, 3,721, and 4,565 m). The bathymetry is as realistic as permitted by the resolution. Further details are given by Toggweiler et al. (1989*a*) and Sarmiento et al. (1992).

The annual mean wind stress of Hellerman and Rosenstein (1983) provides the upper boundary condition to solve the equations of motion, with the vertical velocity, w, set to zero at the air–sea interface to filter out gravity waves. The primary features of the upper ocean circulation, as illustrated by the meridional overturning shown in Fig. 2 and the near-surface vertical velocities shown in Fig. 3a, are the wind-driven Ekman transport, with associated upwelling arising from Ekman divergence in the equatorial and polar gyre regions, and downwelling resulting from Ekman convergence in the subtropical gyre (cf. Gargett 1991).

A linear drag on the horizontal velocity is specified at the bottom, with a no-slip condition applied at lateral boundaries. Temperature and salinity have no flux permitted across any of the boundaries, but in the surface layer the temperature and salinity fields are forced toward the annual mean observed fields of Levitus (1982) with a time scale of 30 d. Subgrid-scale motions are represented by an eddy viscosity (for momentum) of 20 cm^2 s^{-1} in the vertical and 2.5 $\times$ 10^9 cm^2 s^{-1} in the horizontal, a vertical eddy diffusivity (for tracers) which goes from 0.3 cm^{-2} s^{-1} in the upper kilometer to 1.3 cm^{-2} s^{-1} in the deepest layer according to

$$D_z = 0.8 + \frac{1.05}{\pi} \cdot \tanh^{-1}[4.5 \times 10^{-3}(z - 2.5 \times 10^3)],$$

and a horizontal eddy diffusivity that decreases from 1.0 to 0.5 $\times$ 10^7 cm^{-2} s^{-1} from surface to bottom. The ocean circulation model was run for 2,009 yr by Toggweiler et al. (1989*a*) with a time step of $\frac{1}{300}$ yr.

This model has been used by Toggweiler et al. (1989*a,b*) to simulate the oceanic distribution of ^{14}C. They found generally good agreement between simulated and observed distributions. However, the uptake of bomb-produced ^{14}C was somewhat too small, indicating that ventilation of the thermocline is too sluggish. It is difficult in a three-di-

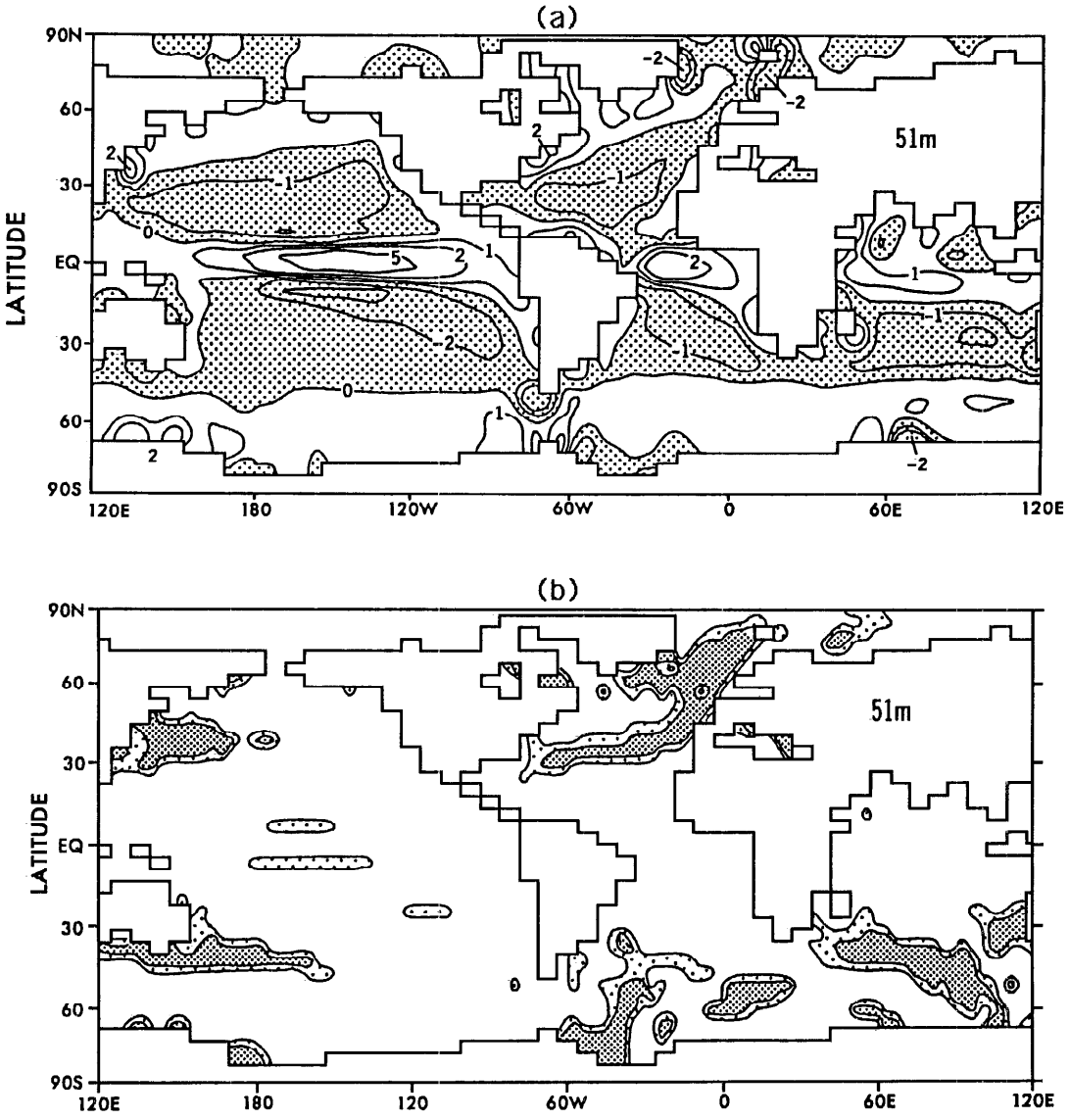

Fig. 3. Vertical advection (a) and convective index (b) at the base of the top layer in the ocean model of Toggweiler et al. (1989*a*). Vertical velocity is given in units of 10^{-6} m s^{-1}; the two contours for the convective index (defined in text) are 25 and 75%.

mensional model of ocean circulation to adjust the vertical exchange, so we use the model being aware of this problem. Further details are given by Toggweiler et al. (1989*a*).

Najjar (1990) ran model P of Toggweiler et al. (1989*a*) for an additional 55 yr to produce time-averaged velocity fields from an average of 17 samplings during the 55-yr run. Our simulations make use of these average velocity fields. Convection in the original model is implemented by stepping down through the water column and homogenizing adjacent layers that are unstable with respect to each other. In many cases it may require several such loops before all instabilities are removed. Rather than allowing an arbitrarily large number of loops, the original model carries out a fixed number

of two loops for each time step. The convection index shown in Fig. 3b was obtained from an average over the entire 55-yr run of the fraction of passes through the convection routine when convection occurs at a given grid point. With 300 time steps per year and two passes through the convection routine per time step, the total 55-yr sample represents 33,000 passes through the convection routine. Convection is most easily dealt with in our off-line model by specifying that it never occurs or that it occurs one pass per time step or two passes per time step. However, the convection index can take on values different than 0, 0.5, and 1.0. We thus follow Najjar's (1990) lead by specifying no convection in our simulation if the convection index is 0 to ⅓, one pass through the convection routine per time step if the convection index is ⅓ to ⅔, and two passes per time step if the index is ⅔ to 1. The resolution and topography of the model are identical to that of Toggweiler et al. (1989*a*), as is the subgrid-scale vertical and horizontal eddy diffusivity.

Gas exchange—In the surface layer we have a contribution to δSMS from gas exchange for CO_2 as well as O_2. The gas exchange contribution is $f_{\delta C}/\Delta z_1$, the perturbation flux of gas divided by the thickness of the first layer of the model. The perturbation flux from atmosphere (atm) to ocean (oc) is given by the following expression

$$f_{\delta C} = k_w\alpha(1 - \gamma_{ice})(\delta pC_{atm} - \delta pC_{oc})$$
$$= k_g(1 - \gamma_{ice})(\delta pC_{atm} - \delta pC_{oc}) \quad (3)$$

with $f_{\delta C}$ in mol m^{-2} yr^{-1}; k_w is the transfer velocity in m yr^{-1}, α the solubility of CO_2 or O_2 in mol m^{-3} ppm^{-1}; k_g the gas-phase-related transfer coefficient in mol m^{-2} yr^{-1} ppm^{-1}, and δpC the perturbation pC in ppm. The annual mean fraction of sea-ice cover, γ_{ice}, is obtained from Alexander and Mobley (1976). The flux through a given grid point in the model is calculated by taking the product of the air–sea difference for that grid point with the average k_g over the entire area represented by the grid point, then correcting the product for the fraction of the area which is covered by ice.

In order to solve Eq. 3 we need to specify k_g, δpC_{atm}, and δpC_{oc}. The windspeed-dependent value for k_g which we use for CO_2 is taken from Sarmiento et al. (1992), who base their k_g on that given by Broecker et al. (1985). Windspeeds are from Esbensen and Kushnir (1981). The global average of this gas exchange coefficient, which is calibrated with the oceanic distribution of bomb ^{14}C, is a little more than twice as large as that given by Liss and Merlivat (1986). We find the bomb-^{14}C calibration to be very compelling, despite recent oceanic measurements with other tracers (Watson et al. 1991) that support the lower gas exchange coefficient of Liss and Merlivat. The study of Sarmiento et al. (1992) shows that uptake of anthropogenic CO_2 by the ocean is reduced by only 11% when the Liss and Merlivat gas exchange coefficient is used because the rate-limiting step for uptake is vertical exchange within the ocean. The perturbation CO_2 uptake we are attempting to simulate occurs in the Southern Ocean, which has a larger vertical exchange than the ocean average. Thus, uncertainty in gas exchange leads to a larger, but still relatively modest uncertainty of ~23% in oceanic uptake, as is shown below.

Temperature dependence of k_g is ignored in the case of CO_2 because the temperature sensitivity of k_w and α for CO_2, which are quite large, approximately cancel when their product is taken. However, this does not apply to O_2. Thus k_g must be modified to take into account the temperature-dependent solubility and diffusivity of O_2. The k_g for CO_2 is divided by the solubility of CO_2 at 20°C to obtain the windspeed-dependent value for k_w that is appropriate for a Schmidt number (Sc) of 600 (the Schmidt number is the molecular diffusivity over the kinematic viscosity). This k_w is multiplied by $(Sc/600)^{-½}$ to correct for the temperature dependence of the molecular diffusivity of O_2 (Liss and Merlivat 1986), then multiplied by the O_2 solubility to obtain k_g. The O_2 solubility and Sc are obtained from the polynomial expressions of Wanninkhof (1992).

δpC_{atm} at the air–sea interface is set to 0 initially for each experiment, then determined as anthropogenic sources are added

to the atmosphere (for CO_2 only), and the ocean is perturbed (for CO_2 and O_2). δpC_{oc} is found from the value for δC obtained by solution of Eq. 2. In the case of O_2, one simply divides δO_2 by the solubility to find δpO_2. CO_2 is more complex, because δC refers to the total carbon content $\delta\Sigma CO_2$, whereas δpC is just the perturbation partial pressure of CO_2, δpCO_2. We follow the approach of Sarmiento et al. (1992) who gave a simple polynomial approximation for the relationship between δpCO_2 and $\delta\Sigma CO_2$. We also include a moist air correction for δpC_{atm}, as discussed by Sarmiento et al. (1992).

The initial value of $pCO_{2\,atm}$ corresponding to $\delta pCO_{2\,atm} = 0$ is 280 ppm. The ocean is assumed to be in equilibrium with 280 ppm when calculating the relationship between δpCO_2 and $\delta\Sigma CO_2$, which means that the relationship is not exact for regions where the ocean and atmosphere are out of equilibrium with each other, such as the equator, where pCO_2 can be as much as 50 ppm or more in excess of atmospheric pCO_2. Our assumption that the error due to this will be small is supported by the comparison discussed by Sarmiento et al. (1992) of their simulation, from which our approach is taken, with the work of Maier-Reimer and Hasselmann (1987) and Bacastow and Maier-Reimer (1990), both of which have an explicit simulation of the preindustrial ocean that includes the aforementioned effects.

Biological uptake and remineralization—We use PO_4^{3-} to simulate biological uptake and remineralization, then calculate the effect of these processes on CO_2 and oxygen by using the Redfield ratios C : P = 130 and $-O_2$: P = 172 (Takahashi et al. 1985). The simulation of Southern Ocean nutrient depletion forces PO_4^{3-} to 0 in the surface ocean. However, we are actually predicting perturbation PO_4^{3-}, i.e. $\delta PO_4^{3-} = PO_4^{3-} - (PO_4^{3-})_0$, where $(PO_4^{3-})_0$ is the initial unperturbed value of PO_4^{3-}. Thus, forcing PO_4^{3-} to 0 is the same as forcing δPO_4^{3-} to $-(PO_4^{3-})_0$. We do this by using a damping term of the form

$$\delta SMS = -\frac{1}{\tau}[\delta PO_4^{3-} + (PO_4^{3-})_0]. \quad (4)$$

A 30-d time scale is used for τ, the same time scale used by Najjar (1990) in predicting new production for his study of oceanic P cycling. The advection-diffusion box model of Joos et al. (1991*a*) depletes nutrients in a surface layer 75 m thick. In order to make our simulation comparable to theirs, we use Eq. 4 in the upper 50.9-m-thick layer of our model, and in the next layer, which is 68.4 m thick, we use Eq. 4 multiplied by (75 m − 50.9 m)/68.4 m = 0.35.

We take 31.12°S as the dividing line south of which surface nutrients are forced toward 0. North of this, we keep the nutrient concentration at its present value, i.e. $\delta PO_4^{3-} = 0$. We accomplish this by using the damping term

$$\delta SMS = -\frac{1}{\tau}(\delta PO_4^{3-}). \quad (5)$$

It will be seen later that the large negative PO_4^{3-} perturbation obtained in surface waters of the Southern Ocean by the nutrient-depletion simulation is advected into the thermocline of the low latitudes. This thermocline anomaly is mixed up to the low-latitude surface ocean, where it has a high probability of giving total surface nutrient contents (present plus anomaly) that are negative because the present nutrient content over most of the low-latitude ocean is already very close to zero. This problem is most readily avoided by forcing the low latitudes to remain in their present, nearly nutrient-depleted state. An alternative, which we did not try, would be to allow the nutrient content to go to zero, but prevent it from becoming negative.

For regeneration we use the expression

$$\delta SMS = \frac{\partial(\delta F)}{\partial z}$$

$$\delta F = \delta F_0 \exp(-z/z^*) \quad (6)$$

below the second layer of the model, i.e. 119.3 m. δF is the perturbation organic P flux, δF_0 is the perturbation organic P flux at the base of the second layer of the model, and $z^* = 800$ m. δF out of the bottom of the ocean is assumed to be 0 (i.e. all organic P that reaches the ocean floor is regenerated

in the bottom box of the ocean). We ignore the small loss to the sediments, which is balanced by a net river input at the surface of the ocean, since it has only a minor impact on the distribution of PO_4^{3-} in the ocean. The choice of an exponential reduction of the organic C flux with a z^* of 800 m is based on the work of Najjar (1990), who found that an expression of this form gave almost as good a fit to the observed PO_4^{3-} field as did his more complex model including dissolved organic P. The inclusion of dissolved organic P in the perturbation model is left for a future study. We examine the sensitivity of the results to different z^* values, as well as to the sediment trap-based scaling for particle fluxes as summarized by Martin et al. (1987):

$$\delta F = \delta F_0 (z/z_e)^{-0.858} \quad (7)$$

where z_e = 119.3 m is the base of the euphotic zone.

A final problem we have is how to deal with areas where anoxia occurs. We determine the existence of anoxia by adding the δO_2 predicted by our model to the observed O_2 field of Levitus (1982). Whenever this indicates anoxia, we continue remineralization of organic C and P according to Eq. 6, but we stop consumption of O_2, assuming NO_3^- provides the electron acceptor and necessary energy for the reaction through the process of denitrification. Denitrification reduces the NO_3^- standing crop of the ocean, unless it is balanced by N_2 fixation at the surface. If denitrification is not balanced by fixation, the resulting loss of NO_3^- from the ocean will reduce the biological pump. The effect of denitrification without any N_2 fixation can be approximated by assuming that the organic P that would otherwise be regenerated in anoxic zones is lost from the ocean. This loss changes the final results by only a few percent over a 100-yr simulation. Our assumption that PO_4^{3-} is regenerated in anoxic zones is equivalent to assuming that denitrification is balanced by N_2 fixation at the surface.

Results

Perturbation new production—Figure 4 shows how new production changes with time as a result of nutrient depletion in the Southern Ocean. There are two major features in the time history of the Southern Ocean. The large initial increase in new production of almost 90 Gt C yr^{-1} results from rapid depletion of nutrients that are in place at present. The 30-d time scale which we use to force the nutrients toward 0 removes these nutrients within a matter of months. This initial pulse is rapidly followed by much lower perturbation new production values of order 14 Gt C yr^{-1}, gradually settling down to ~12 Gt C yr^{-1} after 1,500 yr. It is interesting to compare these increases in new production with estimates of present new production. Eppley's (1989) summary of various estimates for present new production are between 3.4 and 7.4 Gt C yr^{-1}, with an estimate of 20 Gt C yr^{-1} by Packard et al. (1988). Najjar (1990) used the same world ocean model as we did in a series of simulations that gave present new production estimates of between 7 and 13 Gt C yr^{-1}. Najjar's simulation that best agreed with the observations gave a new production of 13 Gt C yr^{-1}. Hence, our Southern Ocean perturbation new production of 12–14 Gt C yr^{-1} represents a doubling of this best estimate.

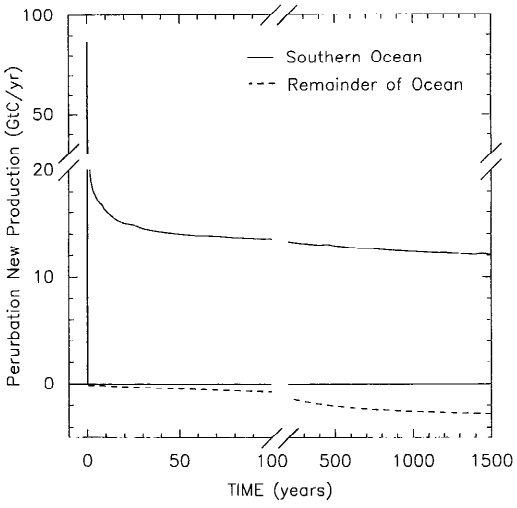

Fig. 4. Time history of perturbed new production in the nutrient-depletion scenario in the Southern Ocean. New production increases in the Southern Ocean region, but is reduced elsewhere.

The high-latitude diffusion-advection (HILDA) model of Joos et al. (1991*a,b*) gives a high-latitude increase in new production

of only 5.5 Gt C yr^{-1} for a scenario similar to ours. The difference between this estimate and ours is a result of the difference in the way the models represent high-latitude processes. Our model has a higher vertical supply of nutrients to the surface.

The increase in new production which is obtained by forcing Southern Ocean nutrients to 0 will continue ad infinitum. There is a continued upward supply of regenerated nutrients that must be removed if surface nutrients are to be kept at 0. If perturbation new production is returned to its prenutrient-depletion scenario value of 0, surface nutrients will climb back to their presimulation values. Taking a median C : Fe molar ratio of 100,000 (average values in cultures range between ~10,000 and ~400,000, e.g. Anderson and Morel 1982; Morel and Hudson 1985; Sunda et al. 1991) gives a requirement of $\sim 0.6 \times 10^6$ t of utilizable Fe per year needed to sustain this enhanced new production. However, substantially more Fe would be required, because after delivery to the ocean, speciation effects (e.g. Bruland et al. 1991) and transport out of the euphotic zone by mixing would render significant amounts unusable.

New production is reduced by a modest amount in regions outside the Southern Ocean (Fig. 4), where nutrients are forced toward their present values. This is due to loss of nutrients from the upper ocean (discussed below).

Figure 5 shows the geographic pattern of perturbed new production that results from the nutrient-depletion scenario after 100 yr. The complex pattern of new production shown is virtually identical to that seen after 1,600 yr of nutrient depletion. Contours in excess of 20 mol of C m^{-2} yr^{-1} are concentrated primarily in regions of convection in the model, with a minor contribution from regions of strong upwelling adjacent to the Antarctic coast (cf. Fig. 3). Given the coarse resolution of the model and the many unrealistic features of the forcing, such as lack of seasonality, it would be unreasonable to expect that the convective overturning in the model would show anything more than a very rough qualitative similarity to the real ocean. Nevertheless, there is a good correlation of the regions of strong convective overturning with topographic and upwelling features that are known to exist in the ocean. The plumes in the southeast Atlantic and southwest Indian Oceans (*see Fig. 3*) are in the vicinity of the Maud Rise Polynya and Cosmonaut Polynya, respectively (Comiso and Gordon 1987). The doming of isopycnal surfaces associated with the Weddell gyre circulation (Gordon 1988) leads to a substantial amount of convective overturning there. The southern Indian Ocean is another region of strong convective activity, in contrast to the South Pacific which has almost no convection (Fig. 3). Gordon et al. (1977) have pointed out that the southern Indian Ocean is a region of particularly strong Ekman upwelling (cf. Fig. 3b). This upwelling would cause a doming of isopycnals which may facilitate convective overturning there.

The model almost certainly does not simulate continental margin processes realistically, such as those involved in the formation of Antarctic Bottom Water. However, we do not expect this failing to have a large effect on the new production pattern of Fig. 5, because most of these areas are ice covered throughout the year. It also means that such areas will not be important for control of atmospheric pCO_2 because they do not come in contact with the atmosphere.

Table 2 includes several studies of the sensitivity of the new production to nutrient depletion in various geographic regions, including a breakdown of the Southern Ocean, as well as the equator, and the North Atlantic and North Pacific Oceans. The breakdown by basins clearly illustrates how anomalous the Pacific Sector of the Southern Ocean is, compared with the Indian as well as the Atlantic Sectors. The Pacific Sector has only 8.3% of the perturbation new production, despite having 41% of the Southern Ocean area. The breakdown by perturbation new production contours at year 100 of the "standard" simulation is even more extreme, with 78% of the perturbation new production concentrated in 18% of the total Southern Ocean area where convection plumes are present.

Nutrient depletion in surface waters of the equatorial region gives a surprising reduction in the perturbation new production of 0.2 Gt C yr^{-1} after 100 yr, by contrast

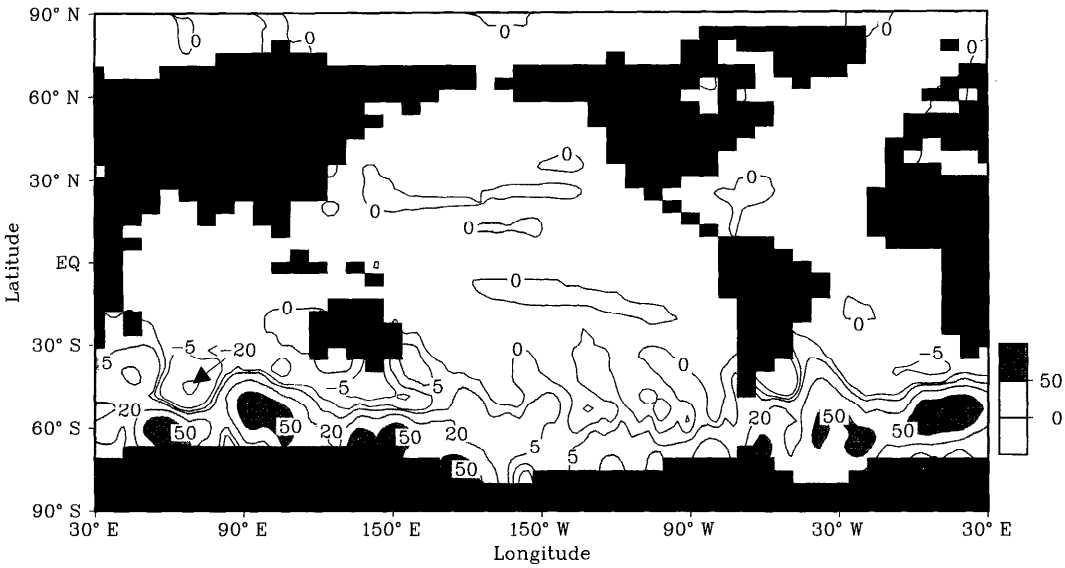

Fig. 5. Map of new production 100 yr after initiation of the Southern Ocean nutrient-depletion scenario; contour intervals are ±5, ±20, and ±50 mol m^{-2} yr^{-1} of C.

with the increase in new production that results from nutrient depletion in the Southern Ocean. The reduction in new production is attributable to the upward supply of nutrients in the equatorial area being supplied primarily by upwelling. Surface nutrient depletion reduces the concentration of nutrients in the upwelling waters and thus the nutrient supply. In the Southern Ocean, upward supply is primarily by convective mixing. The depletion of surface nutrients increases the vertical gradient. Thus the flux by mixing, which is equal to the effective vertical diffusivity (infinite, in the case of convection) times the vertical gradient, increases.

Table 3 shows the sensitivity of the perturbation new production to changes in the

Table 2. Sensitivity of the average atmospheric pCO_2 (ppm) and oceanic O_2 (μmol kg^{-1}) perturbations and total new production (Gt C yr^{-1}) perturbation to the geographic region of nutrient depletion as calculated with the three-dimensional ocean model business-as-usual scenario after 100 yr.

	Depleted of nutrients (%)	Atm. pCO_2 perturbation	Oceanic O_2 perturbation	New production perturbation
North Atlantic (31.12°N–80.06°N)	100	−12.7	−3.1	1.4
North Pacific (31.12°N–66.69°N)	100	−6.9	+1.3	0.4
Equatorial region (17.78°N–17.78°S)	100	−2.8	+2.2	−0.2
Southern Ocean region (south of 31.12°S)	100	−71.8	−15.7	13.2
Breakdown by basins				
Indian Ocean Sector	34	−34.6	−7.8	6.5
Atlantic Ocean Sector	25	−25.1	−5.7	5.6
Pacific Ocean Sector	41	−11.6	−2.3	1.1
Total		−71.3	−15.8	13.2
Breakdown by perturbation new production contours at year 100 (P_{new} in mol C m^{-2} yr^{-1}, cf. Fig. 5)				
$P_{new} \geq 20$	18	−26.8	−9.2	10.3
$0 \leq P_{new} < 20$	39	−19.8	−3.2	1.5
$P_{new} < 0$	43	−21.2	−3.5	1.4
Total		−67.9	−15.9	13.2

Table 3. Sensitivity of the average atmospheric pCO_2 (ppm) and oceanic O_2 (μmol kg^{-1}) perturbations and new production (Gt C yr^{-1}) perturbation to the regeneration length scale z^* in Eq. 6, damping time scale τ in Eq. 4, and gas exchange coefficient in Eq. 3. These are all 100-yr simulations carried out with the three-dimensional ocean model business-as-usual scenario.

	Atm CO_2 perturbation	Oceanic O_2 perturbation	New production perturbation (Gt C yr^{-1})	
			Southern Ocean	Remainder of ocean
Sensitivity to regeneration function (z^* = regeneration length scale)				
z^* = 100 m	−46.3	−6.0	26.5	−1.92
z^* = 800 m (standard)	−71.8	−15.7	14.0	−0.77
z^* = 2,000 m	−80.4	−19.4	9.0	−0.62
z^* = 20,000 m	−85.4	−12.1	5.7	−0.52
Martin et al. (1987) scaling	−67.0	−13.8	17.0	−1.20
Sensitivity to damping time scale (τ)				
τ = 5 d	−85.3	−19.9	29.9	−0.83
τ = 30 d (standard)	−71.8	−15.7	14.0	−0.77
τ = 100 d	−60.5	−11.5	8.2	−0.73
Sensitivity to gas exchange coefficient (k_g in mol m^{-2} yr^{-1} ppm^{-1}; k_g values are averages over the entire ice-free surface area of the model)				
k_g = 0.029 (Liss and Merlivat 1986)	−55.3	−16.1	14.0	−0.77
k_g = 0.065 (standard)	−71.8	−15.7	14.0	−0.77
k_g = 1.2 × standard	−75.5	−15.5	14.0	−0.77
k_g = 2.0 × standard	−84.0	−14.9	14.0	−0.77
Simulation in which the damping terms (Eq. 4 and 5) are applied only in the top layer of the model	−61.7	−12.3	9.4	−0.61

regeneration function and damping time scale (τ), both of which are quantities that are not well constrained by observations, particularly in the Southern Ocean. Deeper regeneration sequesters the perturbation nutrient content out of the reach of convection, thus reducing the absolute magnitude of perturbation new production. In the Southern Ocean this means that perturbation new production goes down with increased regeneration scale depth. In the remainder of the ocean, new production, which is negative, becomes less negative with increased regeneration scale depth. The effect of regeneration length scale on perturbation new production is large—almost a factor of five in the results shown in the table. The Martin et al. (1987) sediment trap-based scaling is intermediate in its effect to the z^* = 100–800-m cases. The regeneration length scale thus has the potential to be a major source of uncertainty in how a nutrient-depletion scenario will affect new production, although it is not as critical in determining atmospheric CO_2 perturbation, as discussed below. The damping time scale also has an impact on perturbation new production which is greater than its impact on atmospheric CO_2 perturbation. A damping time scale of 5 d leads to a large Southern Ocean perturbation new production. The 30-d time scale is insufficient to force nutrients to 0; thus the 5-d time scale produces the larger effect.

PO_4^{3-} perturbation—The perturbation of PO_4^{3-} at the surface due to removal in the region south of 31.12°S is essentially the negative of the observed PO_4^{3-} field shown in Fig. 1. If we were to allow the negative PO_4^{3-} perturbation we impose at the surface to enter the ocean as a passive tracer, in other words, with no regeneration of organic matter, it would penetrate into the Antarctic Intermediate Water in all three ocean basins, as well as into the Circumpolar and Antarctic Bottom Water. With regeneration of organic matter, we see that the addition of PO_4^{3-} below the Southern Ocean regions of organic matter production at the surface overwhelms the negative perturbation in circumpolar and bottom waters (Fig. 6). On the other hand, reduction of nutrients in

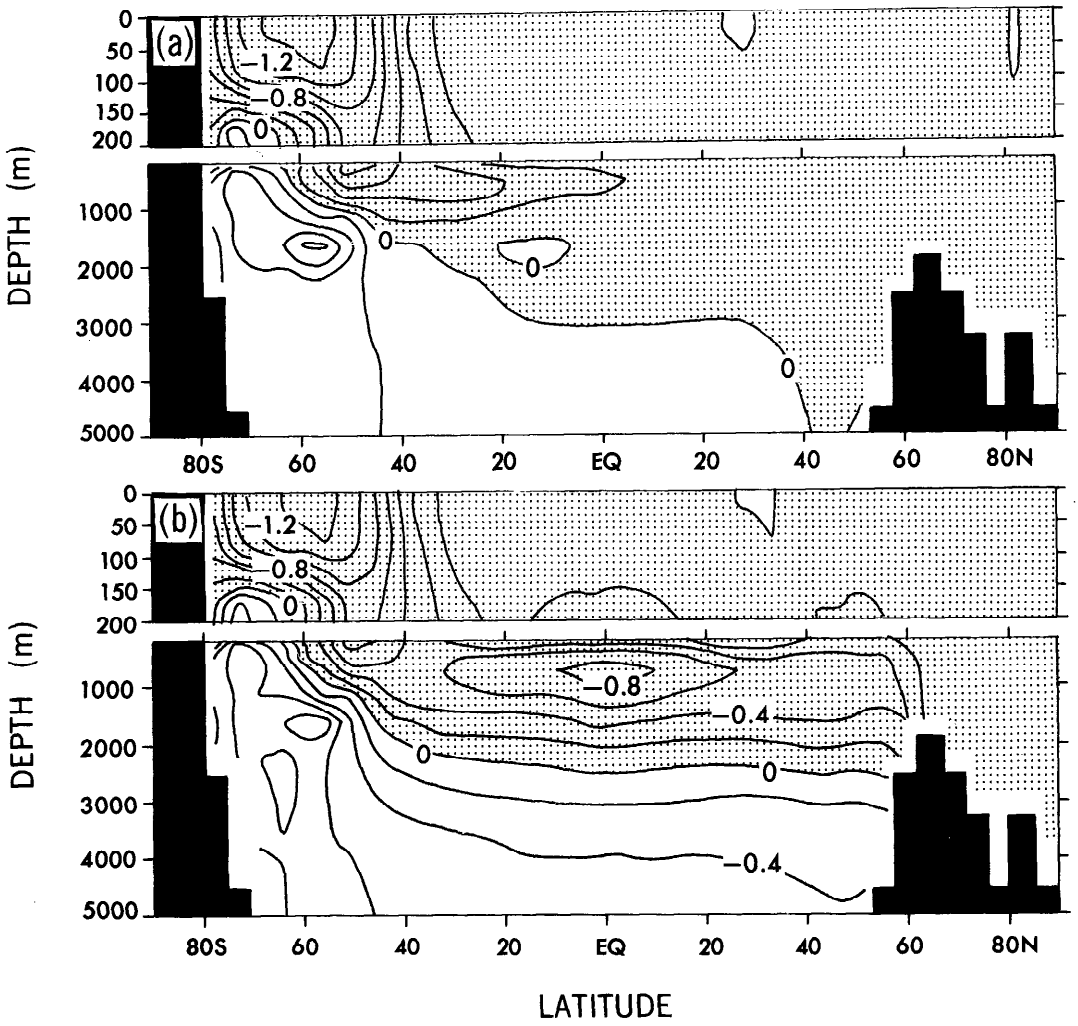

Fig. 6. Global zonal average PO_4^{3-} perturbation sections at 100 yr (a) and 1,600 yr (b) after initiation of the nutrient-depletion scenario; contour interval is 0.2 μmol kg^{-1}.

intermediate and near-surface waters in low latitudes leads to reduction of new production at the surface in those regions. This leads, in turn, to reduction in regeneration of PO_4^{3-} below the surface, which intensifies the negative anomaly of the intermediate waters. Thus, we see that the PO_4^{3-} perturbation consists of four parts: first, the negative Southern Ocean surface anomaly transported in from the surface; second, the positive anomaly added to the water below the surface in the Southern Ocean, which is then also advected into the interior by Antarctic Bottom Water; third, a restoring force in surface low latitudes, equivalent to a reduction in photosynthesis, which forces toward 0 the negative PO_4^{3-} anomaly upwelling from below (i.e. it adds PO_4^{3-}); and fourth, the negative anomaly added to the intermediate waters below the surface in the low latitudes due to the reduced photosynthesis in part three. The basic pattern is already established after 100 yr (Fig. 6a), although it is confined primarily to the southern hemisphere.

The overall result of all these processes is a massive transfer of PO_4^{3-} from intermediate waters to circumpolar and bottom wa-

Table 4. Anthropogenic emissions in the business-as-usual scenario (Houghton et al. 1990). Emission fluxes are interpolated linearly between the values given in the table.

Year	Emission (Gt C yr^{-1})
1990	6.54
1995	6.99
2000	7.65
2005	8.35
2010	8.96
2015	9.65
2020	10.49
2025	11.54
2050	15.19
2075	18.73
2100	22.40

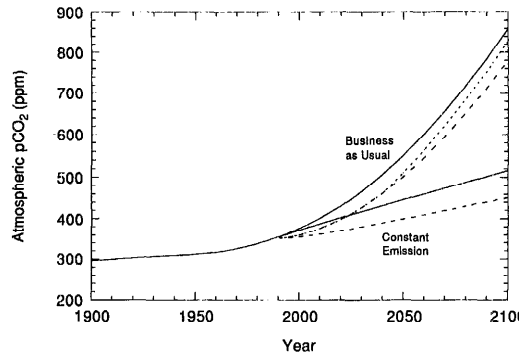

Fig. 7. Atmospheric pCO_2 in the Intergovernmental Panel on Climate Change business-as-usual and constant-emission scenarios. Simulations are shown for cases without nutrient depletion (——), with continuous nutrient depletion (-----), and with 50 yr of nutrient depletion (·····) followed by 60 yr without depletion.

ters. This is very different from the picture that one obtains with the simple three-box ocean models used in previous studies of the ice-age CO_2 reduction (e.g. Toggweiler and Sarmiento 1985). The three-box models have no vertical resolution in the interior, thus they are not able to predict any shift of nutrients in the deep ocean. The scenarios developed with the four-box model of Knox and McElroy (1984), which has one intermediate depth box, all specify an increase in intermediate nutrient concentrations when high-latitude nutrients are depleted. Boyle (1988), on the other hand, had the benefit of Cd data which suggest a downward shift of nutrients during the ice age, so his five-box model for glacial times includes such a downward shift.

Total C and atmospheric pCO_2 *perturbation*—To predict the effect of Southern Ocean nutrient removal on atmospheric CO_2 over the next decades, we need a baseline scenario for how CO_2 might evolve in the absence of such a perturbation because ocean carbon chemistry is sensitive to the atmospheric CO_2 level (Joos et al. 1991*a*,*b*). We start our model with a run for the period 1750 to mid-1990 using the observed atmospheric pCO_2 as did Sarmiento et al. (1992). The combined atmospheric and oceanic increase of the final year of this model (mid-1989 to mid-1990) is 5.88 Gt C yr^{-1}. As with Joos et al. (1991*a*), our standard model projection for increase of atmospheric CO_2 from mid-1990 to mid-2100 is the business-as-usual scenario (Houghton et al. 1990). This scenario increases anthropogenic emissions linearly between the emission rates summarized in Table 4, beginning with an emission of 6.54 Gt C yr^{-1} in 1990 and increasing to a rate of 22.4 in 2100. We also do a constant-emission scenario in which emissions are fixed at their 1990 model-determined level of 5.88 Gt C yr^{-1}. Figure 7 shows a prediction of future atmospheric CO_2 levels which we have made with our three-dimensional ocean circulation model using these two scenarios. Atmospheric CO_2 increases by 430 ppm in the business-as-usual scenario, from its present-day value of 355 ppm to 785 ppm 100 yr from now. In the constant-emission scenario, the 100-yr increase is only 148 ppm.

Figure 8a shows the uptake of atmospheric C by the ocean in the business-as-usual simulation. The uptake in the scenario without nutrient depletion increases with time, from ~2 Gt C yr^{-1} at present to ~6 Gt C yr^{-1} 100 yr from now, as the rate of input of anthropogenic CO_2 to the atmosphere increases. This uptake rate is about a third of the total anthropogenic source to the atmosphere, with about two-thirds staying in the atmosphere. If Southern Ocean nutrients are depleted, the reduced surface pCO_2 that results will enhance the oceanic uptake of anthropogenic CO_2 by 11–12 Gt C yr^{-1} in the first year, decreasing rapidly to be-

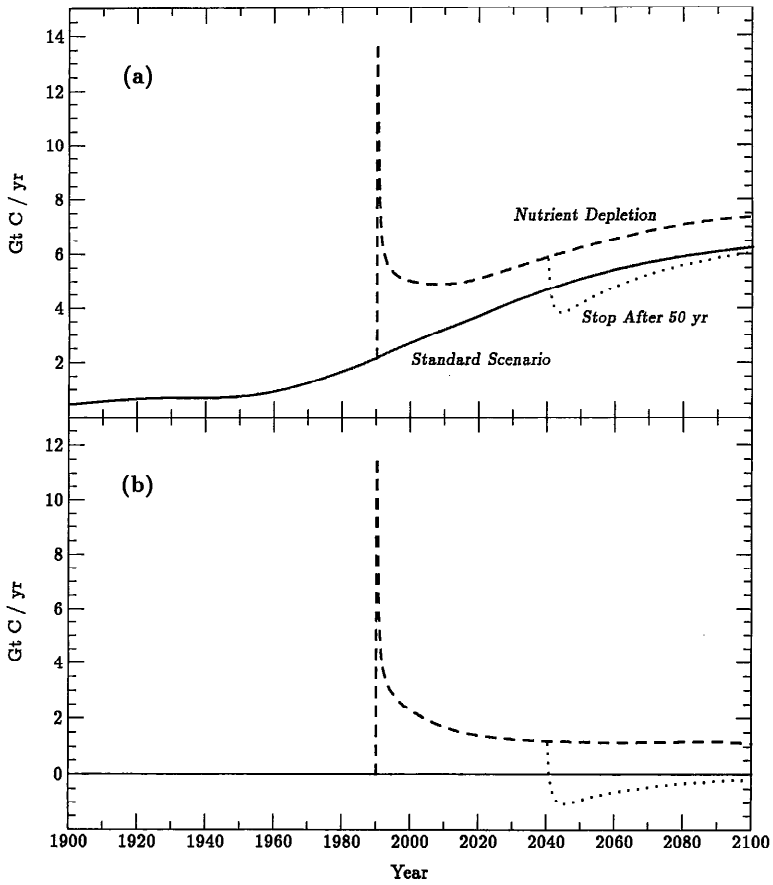

Fig. 8. Fluxes of CO_2 into the ocean in the business-as-usual (standard) scenario without nutrient depletion, with 100 yr of nutrient depletion, and with 50 yr of nutrient depletion followed by 60 yr without depletion. [a.] The total perturbation flux. [b.] Portion of the total flux due to nutrient depletion.

tween 1 and 2 Gt C yr^{-1} (Fig. 8b). The enhancement due to nutrient depletion diminishes to 0 over a time scale of a few millenia, as the deep waters that exchange with surface Southern Ocean waters become charged with sufficient excess CO_2 to make up for the disequilibrium caused by nutrient depletion.

As Table 2 shows, the additional amount of atmospheric pCO_2 removed over the next 100 yr in the business-as-usual nutrient-depletion scenario is 72 ppm (i.e. 152 Gt C), which represents only 16.7% of the total increase of 430 ppm in the business-as-usual scenario with no depletion.

One of the interesting things that a three-dimensional model such as this allows one to do is examine what would happen if nutrients were removed in only certain regions of the ocean. The Pacific equatorial region, where nutrient concentrations are presently high (Fig. 1), is particularly attractive as a site for Fe fertilization because of its accessibility. However, nutrient removal over the entire equatorial band from 17.78°S to 17.78°N gives only a 3 ppm removal of pCO_2 from the atmosphere after 100 yr (Table 2). As pointed out earlier, the reason is that equatorial waters are isolated from the vast bulk of the ocean because of their low density. Nutrient depletion in the North Pacific reduces atmospheric pCO_2 by 7 ppm (Table 2). This depletion is larger than for the equatorial band, presumably because the North Pacific exchanges with a larger volume of water contained in the main thermocline. The relatively small 13-ppm effect of nutrient depletion in the North Atlantic, de-

spite its role as the source of much of the water that fills the deep ocean, is attributable to the fact that the surface nutrient concentration of this area is already low.

The regional scenarios of nutrient depletion in the Southern Ocean, as separated by basins and by the new production contours at year 100 (Table 2), suggest that much of the effect can be obtained by concentrating the nutrient-depletion effort in those areas where the supply of nutrients to the surface is greatest. Thus, the Indian Ocean, with 34% of the area, gives 48% of the total effect. The fertilization of just the 18% of the ocean perched on top of the convective plumes gives 37% of the total signal.

Figure 7 also shows several other scenarios similar to those reported by Joos et al. (1991*a*). The main point when comparing the constant-emission to the business-as-usual scenario is that reduced emissions have a far greater impact on atmospheric CO_2 than does nutrient depletion. Furthermore, the fractional impact of the nutrient-depletion scenario is far greater when emissions are controlled. Also shown in Fig. 7 are scenarios in which nutrient removal is stopped after 50 yr. In this case, excess CO_2 captured by the ocean during the first 50 yr gradually escapes back to the atmosphere during the subsequent 60 yr of the simulation. The effect of nutrient depletion is reversible. The biological pump must maintain surface nutrients and total C at their lower value or CO_2 will escape back to the atmosphere.

Table 3 shows the sensitivity of atmospheric CO_2 to the regeneration function and damping time scale. The longer the regeneration length scale is, the greater the reduction in atmospheric CO_2. The shallow regeneration scenarios take up significantly less CO_2 because the high, shallow CO_2 concentrations that result give a higher average surface pCO_2 content, thus reducing the air–sea CO_2 gradient that drives oceanic uptake. The simulation in which nutrient depletion is done in the top layer only, shown at the bottom of Table 3, has a smaller CO_2 uptake because its average surface pCO_2 content is also higher than the standard case, where nutrient depletion reduces C in the second layer as well. Apparently the nutrient depletion is not sufficiently fast, even with a 30-d time scale, to remove all the nutrients and perturbation total C that are transported to the surface, as is illustrated by the 5-d time-scale simulation, which increases CO_2 uptake by 19% and would presumably show less sensitivity to the regeneration length scale.

Table 3 also shows the result of a series of simulations in which gas exchange was varied over a range similar to that of the studies of gas exchange sensitivity carried out by Sarmiento et al. (1992). A factor-of-two increase in gas exchange gives a 17.0% increase in anthropogenic CO_2 uptake after 100 yr of nutrient depletion. The Liss and Merlivat (1986) gas exchange coefficient gives a 23% reduction in CO_2 uptake. It is generally considered that gas exchange is not limiting to CO_2 uptake in the ocean. Thus, Sarmiento et al. (1992) obtained only a 9.1% increase in anthropogenic CO_2 uptake from doubling the gas exchange coefficient and an 11% reduction with the Liss and Merlivat coefficient in their simulation of the anthropogenic CO_2 uptake from 1750 to 1990. The greater sensitivity of the nutrient-depletion scenario is facilitated by removal of significantly more atmospheric CO_2 in the Southern Ocean, where vertical transport of CO_2 out of the surface is more rapid than in most of the rest of the ocean. Vertical exchange is rapid enough in the Southern Ocean that the gas exchange rate for the nutrient-depletion scenarios is more significant as a limiting factor in oceanic uptake of anthropogenic CO_2.

A drawback of these nutrient-depletion studies is that the model does not include seasonal changes in wind, heat and water exchange, or ice extent. Also, we have not parameterized in any way the influence of seasonal changes in supply of light or changes that result from seasonal variations in thickness of the mixed layer. However, one simulation was performed where the nutrient-depletion δSMS term was set to zero for 6 months of each year; it reduced atmospheric CO_2 removal by 9%, from 72 ppm to 65 in the business-as-usual scenario. The effect is small because the regeneration of organic matter removed from the surface occurs

deep enough that most of it is not mixed back up to the surface during the 6 months when the nutrient-depletion δSMS term is zero. In addition, a simulation was run in which sea ice was eliminated. It impacts the gas exchange and perturbation new production because both are assumed to be 0 under the ice. The CO_2 uptake increased by only 3% (to 74 ppm). The effect is small because most of the relevant processes occur in the open ocean.

Oxygen perturbation—Both Broecker (1990) and Sarmiento (1991) raised the possibility of significant oceanic oxygen reduction in the context of the Fe-fertilization scenario. Joos et al. (1991*b*) carried out a 100-yr simulation of Southern Ocean nutrient depletion with the HILDA model, finding an average reduction of 13 μmol kg^{-1} in all the deep waters except those of the Southern Ocean, where the reduction was 120 μmol kg^{-1}. The reduction in their single high-latitude, deep box is >50% of the present oxygen concentration. More realistic models which resolve the structure of the Southern Ocean would tend to concentrate this oxygen reduction in the upper water. The possibility thus exists that anoxia might develop. Here, we discuss the results of our three-dimensional simulation of oxygen in the Southern Ocean nutrient-depletion scenario.

If there were no gas exchange, the oxygen perturbation would be the mirror image of that of PO_4^{3-} shown in Fig. 6. Oxygen would increase in the intermediate waters, due in part to advection down from the high-latitude surface where it is produced by photosynthesis and in part to the decreased intermediate water regeneration noted in the discussion of the PO_4^{3-} distribution. It would be reduced in the Circumpolar Water and Antarctic Bottom Water, where increased organic C regeneration gives rise to increased oxygen demand. With gas exchange, however, there is a net loss of 15.7 μmol kg^{-1} of oxygen from the ocean after 100 yr and 39.7 after 1,600 yr. The 100-yr signal corresponds to a 9.3% reduction in the average oceanic oxygen content of 168 μmol kg^{-1} and leads to a 0.07% increase in atmospheric oxygen. The removal of oxygen from the ocean would lead one to expect that oceanic oxygen anomalies might be more negative or less positive than PO_4^{3-} perturbation would suggest they should be.

A comparison of the oxygen perturbation distribution of Fig. 9 with the PO_4^{3-} distribution in Fig. 6 supports the overall picture of an anticorrelation between oxygen and PO_4^{3-}. The loss of oxygen to the atmosphere is reflected in the oxygen maximum being smaller than would be predicted from the PO_4^{3-} distribution. For example, the minimum PO_4^{3-} perturbation at 1,600 yr, which occurs in low latitudes (Fig. 6b), is of order -0.8 μmol kg^{-1}, corresponding to a perturbation oxygen maximum of order 140 μmol kg^{-1} when multiplied by the Redfield ratio of -172. The actual maximum oxygen perturbation obtained by the model is less than half this (Fig. 9b). Similarly, the maximum PO_4^{3-} perturbation in the Southern Ocean (Fig. 6b) is of order 0.8 μmol kg^{-1}, corresponding to an oxygen minimum of -140 μmol kg^{-1}, compared with the model prediction of less than -200 μmol kg^{-1}. An important aspect of the oxygen distribution is that this large negative oxygen perturbation in deep waters of the Southern Ocean gives rise to anoxia at middepths south of Africa (Figs. 10 and 11).

The major surprise of the three-dimensional oxygen simulations is that the loss of oxygen in the 1,600-yr Southern Ocean nutrient-depletion scenario is far smaller than that obtained by box model studies such as those of Knox and McElroy (1984), Toggweiler and Sarmiento (1985), and Sarmiento et al. (1988). Our model loses only 39.7 μmol kg^{-1} of oxygen after 1,600 yr of nutrient depletion, compared with, for example, a loss of 144 μmol kg^{-1} in the three-box model simulation of Toggweiler and Sarmiento (1985). The average oxygen content of the ocean is $\sim$168 μmol kg^{-1}, so the three-box model scenario drives the ocean nearly to complete anoxia. This difference in the models occurs despite the fact that PO_4^{3-} removal from the Southern Ocean surface is higher in the three-dimensional model (0.95 μmol kg^{-1} in the upper two layers where nutrient depletion occurs) than in the three-box model (0.77 μmol kg^{-1}).

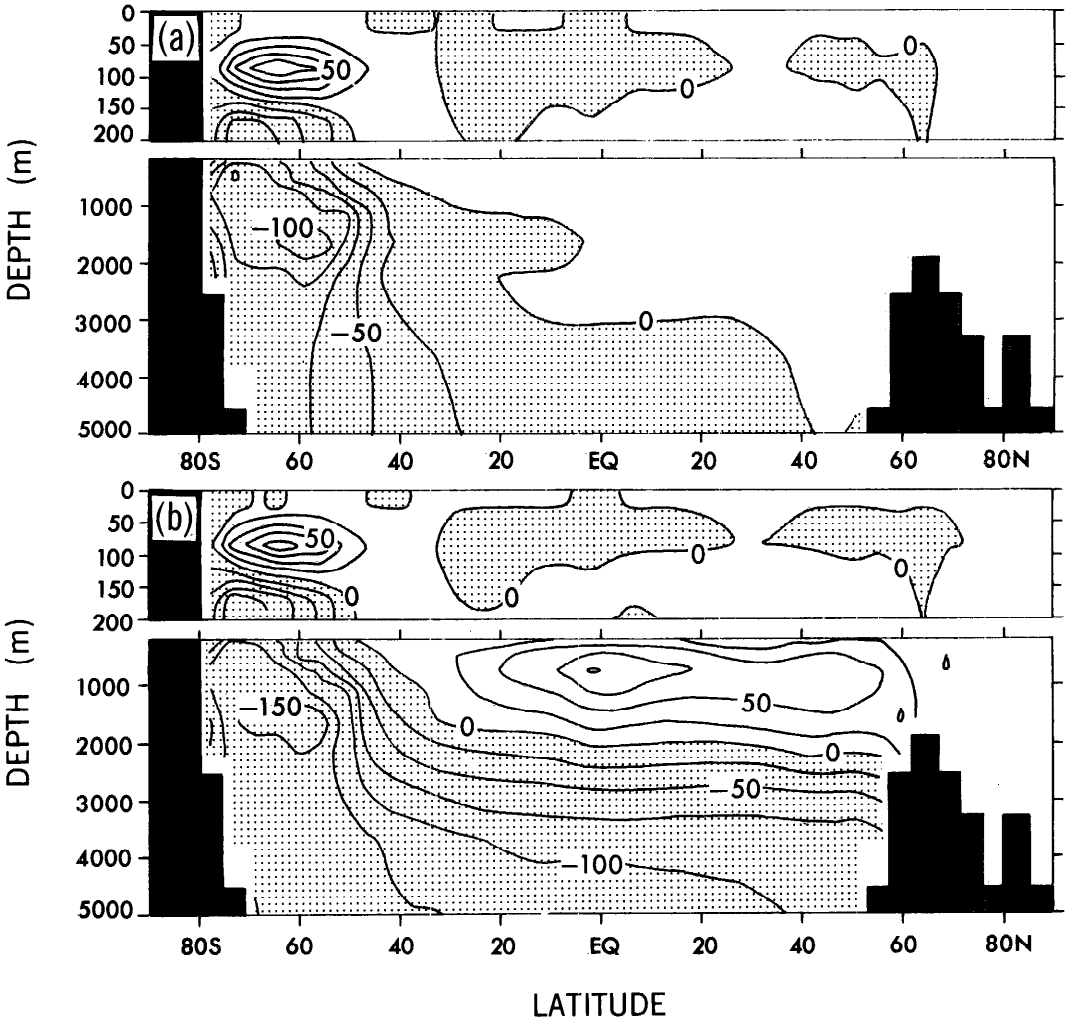

Fig. 9. Global zonal mean north–south oxygen perturbation sections at year 100 (a) and year 1,600 (b); contour interval is 25 μmol kg^{-1}.

Why is there such a difference in the oxygen distribution predicted by these simulations? An analysis of the fate of oxygen produced by increased Southern Ocean photosynthesis provides the answer.

The photosynthetic production of oxygen resulting from nutrient depletion in surface waters of the Southern Ocean is 157.94 × 10^{13} mol yr^{-1} after a 1,600-yr simulation (Table 5). The regeneration of organic matter produced by this photosynthesis leads to an exactly equivalent oxygen demand in the deep ocean. In order to achieve a steady state, the photosynthetic oxygen must be transported into the deep ocean at the same rate at which it forms. The ocean is not quite in steady state after 1,600 yr, but it is close, with a net loss of only 1.05 × 10^{13} mol yr^{-1} from the ocean to the atmosphere. One way of achieving increased transport of oxygen into the deep ocean would be by increasing surface oxygen concentration. However, surface oxygen concentration is forced by rapid gas exchange to be close to saturation with the atmosphere. The atmospheric reservoir of oxygen is so much larger than that of the ocean that this constraint requires, in effect, that

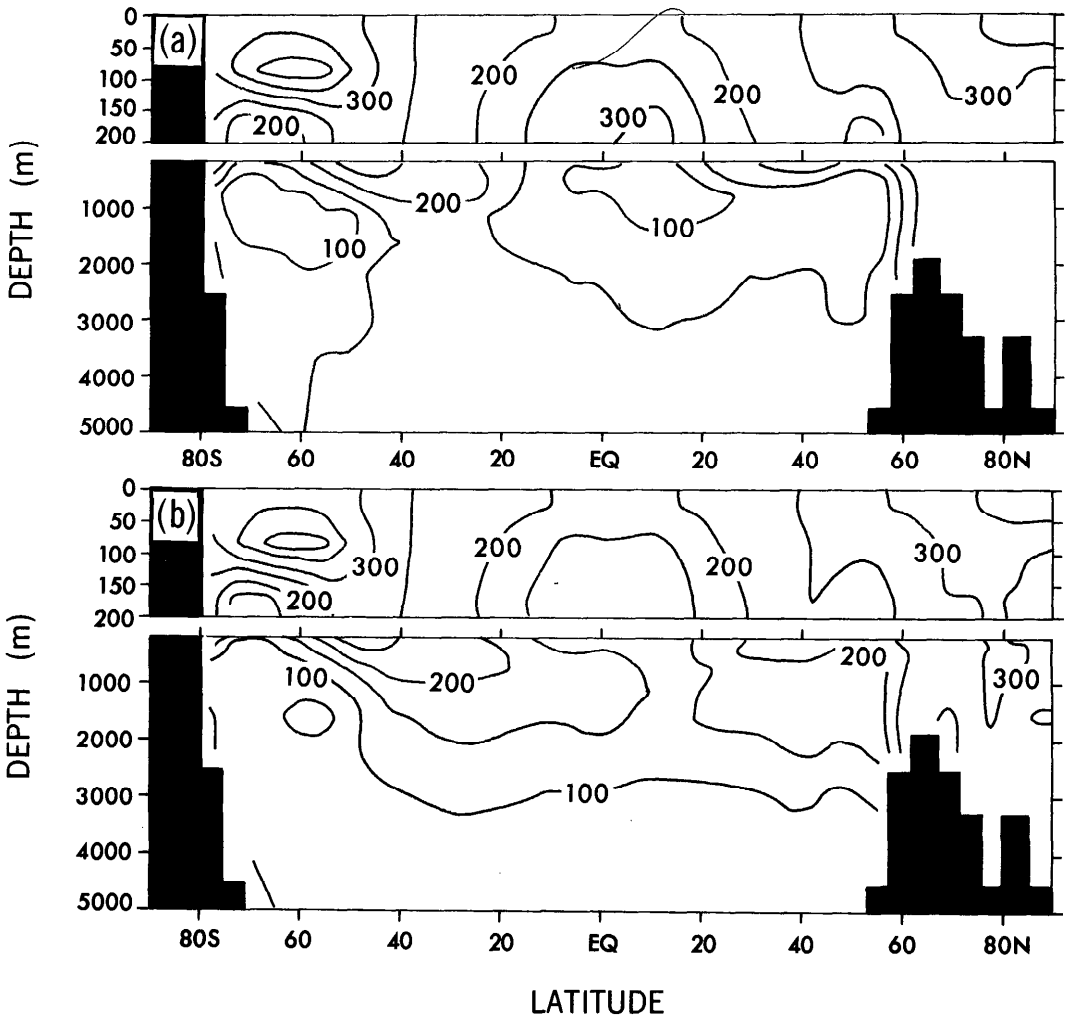

Fig. 10. Global zonal mean oxygen perturbation + observations sections at year 100 (a) and year 1,600 (b); contour interval is 50 μmol kg^{-1}.

surface oxygen concentration remain close to its initial value before nutrient depletion. Thus, the primary mechanism by which oxygen transport to the deep ocean can be increased significantly without changing ocean circulation is by reducing the average deep-ocean concentrations. Box models such as that of Toggweiler and Sarmiento (1985) accomplish the required deep-ocean oxygen reduction by displacing oxygen from the entire deep ocean to the atmosphere because the deep ocean is represented by a single box. The three-dimensional model can accomplish the same goal by reducing oxygen in waters just below the surface in the Southern Ocean (cf. Fig. 9). The processes occurring in the remainder of the ocean (*see below*) are such as to increase the oxygen content of intermediate depth waters below the surface (Fig. 9). The total loss in the three-dimensional model is thus much less than in the three-box model.

The above argument needs to be qualified by pointing out that vertical mixing of the two layers in which nutrient damping is carried out is not efficient enough to bring the oxygen content of the second layer into equilibrium with the atmosphere. The sec-

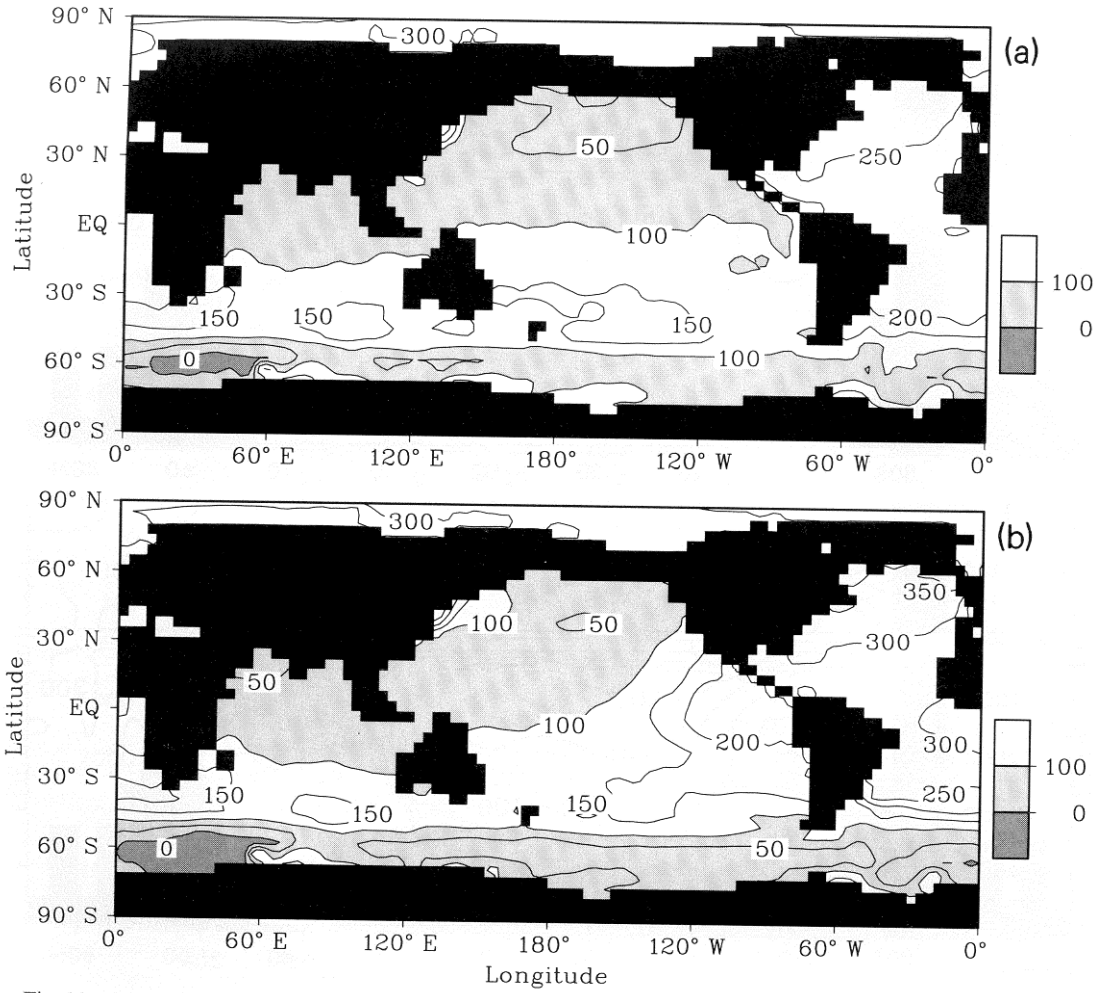

Fig. 11. Map of oxygen perturbation + observations at 1,622 m at year 100 (a) and year 1,600 (b); contour interval is 50 μmol kg^{-1}. Note the appearance of anoxia in the southwestern Indian Ocean.

ond layer thus has quite high oxygen perturbation values in the Southern Ocean, as can be noted by examination of the upper part of the water column in Fig. 9. Tables 3 and 5 show the results of a simulation in which the nutrient damping term was applied in only the top layer of the model. The photosynthetic production of oxygen in the Southern Ocean is reduced by 33%. The loss of oxygen from the deep ocean after 1,600

Table 5. Budget of oxygen perturbation in units of 10^{13} mol yr^{-1}. The standard simulation has Southern Ocean nutrient depletion in the top two layers, as described in the text. The results in the final column are for a simulation in which nutrient depletion was done only in the top layer.

Region	Process	100-yr simulation	1,600-yr simulation	
			Standard	Top layer only
Southern Ocean	New production	153.74	157.94	106.09
	Air–sea flux	−16.03	−8.93	−7.91
Remainder of ocean	New production	−8.45	−27.86	−23.18
	Air–sea flux	4.66	7.88	6.90
Atmosphere	Rate of increase	11.37	1.05	1.01

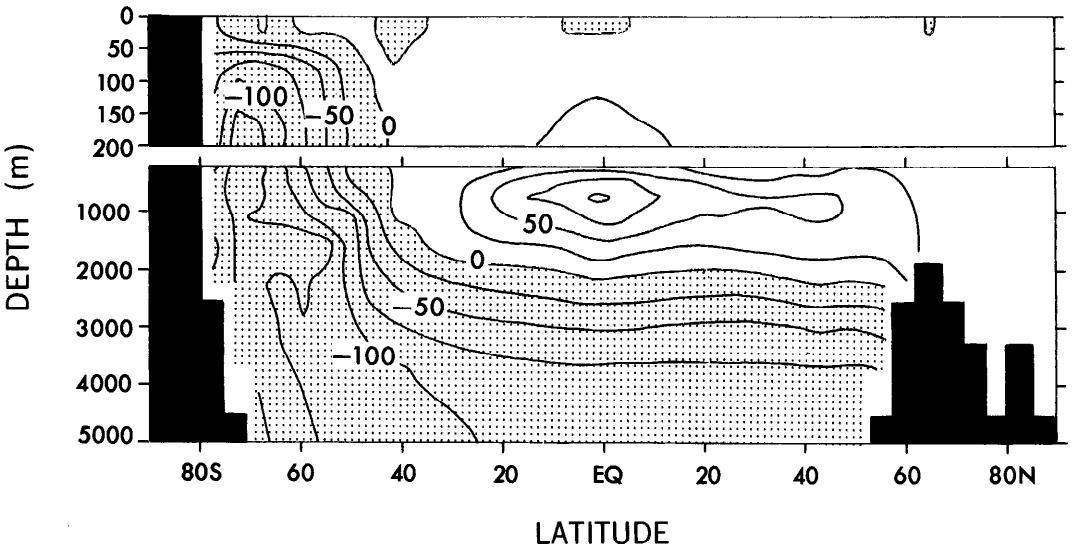

Fig. 12. Global zonal mean north–south oxygen perturbation at year 1,600 of a simulation in which the nutrient-damping terms (Eq. 4 and 5) were applied only in the top layer of the model; contour interval is 25 μmol kg^{-1}.

yr is now only 31.2 μmol kg^{-1}, as compared with 39.7 μmol kg^{-1} for the standard simulation. The 100-yr simulation loses 12.3 μmol kg^{-1}, as compared with 15.7 μmol kg^{-1} in the standard simulation. The smaller oxygen loss is most likely due to the fact that vertical exchange between the top two layers of the model is more efficient than between the second and third layers. The vertical gradient required to remove photosynthetic oxygen from the surface is thus smaller. The effect on the oxygen distribution is very noticeable, as can be seen by comparing Figs. 9b with 12.

Another way to get rid of oxygen produced in surface waters of the Southern Ocean would be by loss at the air–sea interface balanced by a gain in the atmosphere and the rest of the ocean. However, air-sea exchange can only account for 8.93×10^{13} mol yr^{-1} of the required sink (Table 5). Thus, the most important sink for photosynthetic oxygen is by downward transport within the Southern Ocean. The remainder of the ocean has, on average, a reduced photosynthetic production of oxygen. The reduced photosynthetic production of organic C plays a role in increasing the oxygen content in the intermediate depth waters (Fig. 9). The increased intermediate depth oxygen content results in an upward vertical transport of oxygen (Table 5) which is the main source of oxygen required to balance the surface perturbation sink.

The small loss of oxygen in the three-dimensional model simulation has important implications for the high-latitude nutrient-depletion hypothesis as an explanation for the ice-age pCO_2 observations. The low levels of oxygen predicted by the three-box model, high-latitude nutrient-depletion scenario should have had a major impact on sediment properties. No evidence of such an impact has been found. Now it appears that the box model predictions are incorrect due to a lack of vertical resolution in the ocean interior.

The sensitivity of the oxygen loss to regeneration length scale (Table 3) results from the fact that shallower regeneration greatly increases the efficiency of oceanic mixing in removing the surplus oxygen produced at the surface, thus preventing loss of oxygen to the atmosphere. The increased oxygen loss with the 5-d damping time scale (*see Table 3*) results from the increased oxygen production rate that one can infer from the increased new production. Getting rid of this oxygen requires a steeper gradient in the ocean, which can only be satisfied by removing more oxygen from the ocean. The longer regeneration time scales, with their

Table 6. Summary of standard model estimates for the average change in atmospheric pCO_2 for 100-yr simulations of the effect of Southern Ocean surface nutrient depletion. The percent of total increase is given relative to the increase that occurs in a simulation without nutrient removal. The range given in parentheses for the business-as-usual scenario is taken from the sensitivity studies shown in Table 3.

	Atmospheric CO_2 perturbation (ppm)		
	This study	Joos et al. 1991*a,b*	% of total increase
Business-as-usual	−72 (−46 to −85)	−107	17–26
Constant emission	−61	−90	42–60

lower perturbation new production, require less of a vertical gradient, and thus lower O_2 loss from the ocean. The low sensitivity of oxygen loss to gas exchange (*see Table 3*) results because air–sea exchange of oxygen is not a rate-limiting step, since it is already very rapid, and most of the adjustment that needs to take place is within the ocean, as we have already seen.

Discussion

Combining the results of our standard business-as-usual and constant-emission, three-dimensional simulations with the results of the earlier box model studies of Joos et al. (1991*a,b*) gives the summary shown in Table 6. In the business-as-usual scenario, nutrient depletion removes ~20% of the total increase of CO_2 over the next 100 yr. The sensitivity studies summarized in Table 3 give a range of −46 to −85 ppm for our −72 ppm standard simulation. In a constant-emission scenario which fixes anthropogenic CO_2 emissions at their present levels of nearly 6 Gt C yr^{-1}, the enhanced oceanic uptake due to nutrient depletion is ~50% of the total increase. The result we obtain with our three-dimensional model is comparable to the numbers which Peng and Broecker (1991*a*) found with their bomb-^{14}C-calibrated box model study, but somewhat smaller than Joos et al. obtained in their box model study. Joos et al. used bomb ^{14}C to calibrate their model as well, but they did not use the deep, high-latitude ^{14}C, arguing that bomb-^{14}C data were insufficient to properly constrain the model in that area. Instead, they validated the vertical and horizontal exchange of the deep, high-latitude waters with chlorofluorocarbon observations. The lower uptake of our three-dimensional model is consistent with its underestimate for the global uptake of bomb ^{14}C (Toggweiler et al. 1989*b*).

The uptakes summarized in Table 6 are large. It should be emphasized, however, that these nutrient-depletion scenarios are extreme cases of almost instantaneous complete nutrient depletion within the surface waters of the Southern Ocean. It seems unlikely that such a scenario could be achieved in practice. We have ignored such things as the fact that the iron limitation hypothesis is still controversial (e.g. Banse 1991), the suggestions by various investigators that light limitation by deep summertime mixed layers, cloud cover, and wintertime darkness may be of greater importance than micronutrient supply (e.g. Mitchell et al. 1991; Nelson and Smith 1991), and the impact of zooplankton grazing on the phytoplankton standing crop (e.g. Frost 1991). Clearly, all of these issues need to be addressed by further observational and model studies.

In addition, the impacts of a nutrient-depletion scenario require careful examination before serious application of this idea. We have demonstrated that oceanic oxygen would be reduced by 15.7 (6.0–19.9) μmol kg^{-1}, with anoxia resulting in the southwestern Indian Ocean. This would have a dramatic effect on ocean biology and chemistry in that region. Fuhrman and Capone (1991) outlined a series of other issues that need to be addressed, such as the extent to which the anoxia might result in significant CH_4 production, the potential for a self-fertilization effect due to mobilization of Fe in anoxic sediments, and the effect of enhanced oceanic production on dimethylsulfide and nitrous oxide production. In addition, it is clear that the increase of 13.2 (5.2–29.1) Gt C yr^{-1} in oceanic production of organic matter concentrated in an area

that covers ~16% of the world ocean would have dramatic effects on oceanic ecology which are difficult to predict.

There seems no reason to modify the conclusions of Broecker (1990) and Sarmiento (1991) that it is unlikely that the Fe fertilization strategy will achieve practical application. On the other hand, the scientific issues involved in evaluating the idea are important ones that relate to how the ocean carbon cycle functions, as well as to how the ice-age reduction in CO_2 may have occurred, and how the oceans might respond to future changes in circulation and biology that will result from greenhouse warming. It is thus important that we continue to further our understanding of what controls the biological pump in the Southern Ocean and how it affects atmospheric CO_2 as well as the distribution of other chemical species in the ocean and atmosphere.

References

ALEXANDER, R. C., AND R. L. MOBLEY. 1976. Monthly average sea surface temperatures and ice pack limits on a 1° global grid. Monthly Weather Rev. **104:** 143–148.

ANDERSON, M. A., AND F. M. M. MOREL. 1982. The influence of aqueous iron chemistry on the uptake of iron by a coastal diatom *Thalassiosira weissflogii*. Limnol. Oceanogr. **27:** 789–813.

BACASTOW, R., AND E. MAIER-REIMER. 1990. Ocean-circulation model of the carbon cycle. Clim. Dyn. **4:** 95–125.

BAES, C. F., AND G. G. KILLOUGH. 1986. Chemical and biological processes in CO_2-ocean models, p. 329–347. *In* J. R. Trabalka and D. E. Reichle [eds.], The changing carbon cycle. Springer.

BANSE, K. 1991. Rates of phytoplankton cell division in the field and in iron enrichment experiments. Limnol. Oceanogr. **36:** 1886–1898.

BOYLE, E. A. 1988. The role of vertical fractionation in controlling Late Quaternary atmospheric carbon dioxide. J. Geophys. Res. **93:** 15,701–15,714.

BROECKER, W. S. 1982. Ocean chemistry during glacial time. Geochim. Comochim. Acta **46:** 1689–1705.

———. 1990. Comment on "iron deficiency limits phytoplankton growth in Antarctic waters" by John H. Martin et al. Global Biogeochem. Cycles **4:** 3–4.

———, AND T.-H. PENG. 1982. Tracers in the sea. Eldigio.

———, AND ———. 1989. The cause of the glacial to interglacial atmospheric CO_2 change: A polar alkalinity hypothesis. Global Biogeochem. Cycles **3:** 215–240.

———, ———, G. ÖSTLUND, AND M. STUIVER. 1985. The distribution of bomb radiocarbon in the ocean. J. Geophys. Res. **90:** 6953–6970.

BRULAND, K. W., J. R. DONAT, AND D. A. HUTCHINS. 1991. Interactive influences of bioactive trace metals on biological production in oceanic waters. Limnol. Oceanogr. **36:** 1555–1577.

BRYAN, K. 1969. A numerical method for the study of the circulation of the world ocean. J. Comput. Phys. **4:** 347–376.

COMISO, J. C., AND A. L. GORDON. 1987. Recurring polynyas over the Cosmonaut Sea and the Maud Rise. J. Geophys. Res. **92:** 2819–2833.

CULLEN, J. 1991. Hypotheses to explain high nutrient conditions in the open sea. Limnol. Oceanogr. **36:** 1578–1599.

EPPLEY, R. W. 1989. New production: History, methods, problems, p. 85–97. *In* W. H. Berger et al. [eds.], Productivity of the ocean: Present and past. Wiley.

ESBENSEN, S. K., AND Y. KUSHNIR. 1981. The heat budget of the global ocean: An atlas based on estimates from surface marine observations. Oregon State Univ. Clim. Res. Inst. Rep. 29.

FROST, B. 1991. The role of grazing in nutrient-rich areas of the open sea. Limnol. Oceanogr. **36:** 1616–1630.

FUHRMAN, J. A., AND D. G. CAPONE. 1991. Possible biogeochemical consequences of ocean fertilization. Limnol. Oceanogr. **36:** 1951–1959.

GARGETT, A. E. 1991. Physical processes and the maintenance of nutrient-rich euphotic zones. Limnol. Oceanogr. **36:** 1527–1545.

GORDON, A. L. 1988. Spatial and temporal variability within the Southern Ocean, p. 41–56. *In* D. Sahrhage [ed.], Antarctic Ocean and resources variability. Springer.

———, H. W. TAYLOR, AND D. T. GEORGIE. 1977. Antarctic oceanographic zonation, p. 45–76. *In* Polar oceans. Conf. Proc. Arct. Inst. North Am.

HELLERMAN, S., AND M. ROSENSTEIN. 1983. Normal monthly wind stress over the world ocean with error estimates. J. Phys. Oceanogr. **13:** 1093–1104.

HOUGHTON, J. T., G. J. JENKINS, AND J. J. EPHRAUMS. 1990. Climate change: The IPCC scientific assessment. Cambridge.

JOOS, F., J. L. SARMIENTO, AND U. SIEGENTHALER. 1991*a*. Estimates of the effect of Southern Ocean iron fertilization on atmospheric CO_2 concentrations. Nature **349:** 772–775.

———, U. SIEGENTHALER, AND J. L. SARMIENTO. 1991*b*. Possible effects of iron fertilization in the Southern Ocean on atmospheric CO_2 concentration. Global Biogeochem. Cycles **5:** 135–150.

KNOX, F., AND M. MCELROY. 1984. Changes in atmospheric CO_2: Influence of the marine biota at high latitudes. J. Geophys. Res. **89:** 4629–4637.

LEVITUS, S. 1982. Climatological atlas of the World Ocean. NOAA Prof. Pap. 13. U.S. GPO.

LISS, P., AND L. MERLIVAT. 1986. Air-sea gas exchange rates: Introduction and synthesis, p. 113–128. *In* P. Buat-Menard [ed.], The role of air-sea exchange in geochemical cycling. Reidel.

MAIER-REIMER, E., AND K. HASSELMANN. 1987. Transport and storage of CO_2 in the ocean—an inorganic ocean-circulation cycle model. Clim. Dyn. **2:** 63–90.

MARTIN, J. H. 1990. Glacial-interglacial CO_2 change: The iron hypothesis. Paleoceanography **5:** 1–13.

———, S. E. FITZWATER, AND R. M. GORDON. 1990*a*. Iron deficiency limits phytoplankton growth in Antarctic waters. Global Biogeochem. Cycles **4:** 5–12.

———, R. M. GORDON, AND S. E. FITZWATER. 1990*b*. Iron in Antarctic waters. Nature **345:** 156–158.

———, G. A. KNAUER, D. M. KARL, AND W. W. BROENKOW. 1987. VERTEX: Carbon cycling in the northeast Pacific. Deep-Sea Res. **34:** 267–285.

MITCHELL, B. G., E. A. BRODY, O. HOLM-HANSEN, C. MCCLAIN, AND J. BISHOP. 1991. Light limitation of phytoplankton biomass and macronutrient utilization in the Southern Ocean. Limnol. Oceanogr. **36:** 1662–1677.

MOREL, F. M., AND R. J. HUDSON. 1985. The geobiological cycle of trace elements in aquatic systems: Redfield revisited, p. 251–270. *In* W. Stumm [ed.], Chemical processes in lakes. Wiley.

NAJJAR, R. G. 1990. Simulations of the phosphorus and oxygen cycles in the world ocean using a general circulation model. Ph.D. thesis, Princeton Univ.

NEFTEL, A., E. MOOR, H. OESCHGER, AND B. STAUFFER. 1985. Evidence from polar ice cores for the increase in atmospheric CO_2 in the past two centuries. Nature **315:** 45–47.

NELSON, D. M., AND W. O. SMITH, JR. 1991. Sverdrup revisited: Critical depth, maximum chlorophyll levels, and the control of Southern Ocean productivity by the irradiance-mixing regime. Limnol. Oceanogr. **36:** 1650–1661.

PACKARD, T. T., M. DENIS, M. RODIER, AND P. GARFIELD. 1988. Deep-ocean metabolic CO_2 production: Calculations from ETS activity. Deep-Sea Res. **35:** 371–382.

PENG, T.-H., AND W. S. BROECKER. 1991*a*. Dynamic limitations on the Antarctic iron fertilization strategy. Nature **349:** 227–229.

———, AND ———. 1991*b*. Factors limiting the reduction of atmospheric CO_2 by iron fertilization. Limnol. Oceanogr. **36:** 1919–1927.

SARMIENTO, J. L. 1991. Slowing the buildup of fossil CO_2 in the atmosphere by iron fertilization: A comment. Global Biogeochem. Cycles **5:** 1–2.

———, T. D. HERBERT, AND J. R. TOGGWEILER. 1988. Causes of anoxia in the world ocean. Global Biogeochem. Cycles **2:** 115–128.

———, J. C. ORR, AND U. SIEGENTHALER. 1992. A perturbation simulation of CO_2 uptake in an ocean general circulation model. J. Geophys. Res. **97:** In press.

———, AND J. R. TOGGWEILER. 1984. A new model for the role of the oceans in determining atmospheric pCO_2. Nature **308:** 621–624.

———, ———, AND R. NAJJAR. 1988. Ocean carbon cycle dynamics and atmospheric pCO_2. Phil. Trans. R. Soc. Ser. A **325:** 3–21.

SIEGENTHALER, U., AND T. WENK. 1984. Rapid atmospheric CO_2 variations and ocean circulation. Nature **308:** 624–625.

SUNDA, W. G., D. G. SWIFT, AND S. A. HUNTSMAN. 1991. Low iron requirement for growth in oceanic phytoplankton. Nature **351:** 55–57.

TAKAHASHI, T., W. S. BROECKER, AND S. LANGER. 1985. Redfield ratio estimates based on chemical data from isopycnal surfaces. J. Geophys. Res. **90:** 6907–6924.

TOGGWEILER, J. R., K. DIXON, AND K. BRYAN. 1989*a*. Simulations of radiocarbon in a coarse-resolution world ocean model. 1. Steady state prebomb distributions. J. Geophys. Res. **94:** 8217–8242.

———, ———, AND ———. 1989*b*. Simulations of radiocarbon in a coarse-resolution, world ocean model. 2. Distributions of bomb-produced ^{14}C. J. Geophys. Res. **94:** 8243–8264.

———, AND J. L. SARMIENTO. 1985. Glacial to interglacial changes in atmospheric carbon dioxide: The critical role of ocean surface water in high latitudes. Geophys. Monogr. 32, p. 163–184.

VOLK, T., AND M. I. HOFFERT. 1985. Ocean carbon pumps: Analysis of relative strengths and efficiencies in ocean-driven atmospheric CO_2 changes. Geophys. Monogr. 32, p. 99–110.

WANNINKHOF, R. 1992. Relationship between wind speed and gas exchange over the ocean. J. Geophys. Res. **97:** In press.

WATSON, A. J., R. C. UPSTILL-GODDARD, AND P. S. LISS. 1991. Air-sea gas exchange in rough and stormy seas measured by a dual-tracer technique. Nature **349:** 145–147.

WEISS, R. F. 1974. Carbon dioxide in water and sea water: The solubility of a non-ideal gas. Mar. Chem. **2:** 203–215.

WENK, T. 1985. Einflüsse der Ozeanzirkulation und der marinen biologie auf die atmosphärische CO_2-konzentration, Ph.D. thesis, Univ. Bern.